Molecular Cell
Article

Neuronal MeCP2 Is Expressed at Near Histone-Octamer Levels and Globally Alters the Chromatin State

Peter J. Skene,[1] Robert S. Illingworth,[1] Shaun Webb,[1] Alastair R.W. Kerr,[1] Keith D. James,[2] Daniel J. Turner,[2] Rob Andrews,[2] and Adrian P. Bird[1,*]
[1]Wellcome Trust Centre for Cell Biology, University of Edinburgh, Edinburgh EH9 3JR, UK
[2]Wellcome Trust Sanger Institute, Hinxton, Cambridge CB10 1SA, UK
*Correspondence: a.bird@ed.ac.uk
DOI 10.1016/j.molcel.2010.01.030

SUMMARY

MeCP2 is a nuclear protein with an affinity for methylated DNA that can recruit histone deacetylases. Deficiency or excess of MeCP2 causes severe neurological problems, suggesting that the number of molecules per cell must be precisely regulated. We quantified MeCP2 in neuronal nuclei and found that it is nearly as abundant as the histone octamer. Despite this high abundance, MeCP2 associates preferentially with methylated regions, and high-throughput sequencing showed that its genome-wide binding tracks methyl-CpG density. MeCP2 deficiency results in global changes in neuronal chromatin structure, including elevated histone acetylation and a doubling of histone H1. Neither change is detectable in glia, where MeCP2 occurs at lower levels. The mutant brain also shows elevated transcription of repetitive elements. Our data argue that MeCP2 may not act as a gene-specific transcriptional repressor in neurons, but might instead dampen transcriptional noise genome-wide in a DNA methylation-dependent manner.

INTRODUCTION

Mammalian genomes exhibit tissue-specific patterns of DNA methylation, predominantly at the dinucleotide sequence CpG. In most tissues, the bulk genome has a relatively low CpG density, but is heavily (~70%) methylated (Ehrlich et al., 1982). This global distribution is interrupted by regions of high CpG density, termed CpG islands (CGIs), which are typically unmethylated and associated with gene promoters (Bird et al., 1985). The effects of methylated and nonmethylated CpGs on chromatin metabolism are mediated by proteins that are either attracted or repelled by that modification state. MeCP2 is one of several proteins that bind methylated DNA in vivo and in vitro and is therefore a potential interpreter of the DNA methylation pattern (Lewis et al., 1992). MeCP2 is most highly expressed in the brain, specifically in neurons (Kishi and Macklis, 2004), where neuronal expression rises postnatally as the final stages of neurogenesis are completed (Balmer et al., 2003).

Mutations in the X-linked *MECP2* gene are the primary cause of the autism spectrum disorder Rett syndrome (Amir et al., 1999). In Rett patients, apparently normal development gives way to regression after 6–12 months, with loss of acquired skills, including speech and mobility (Armstrong, 2002). The *Mecp2* null mouse recapitulates several features of Rett syndrome, showing a late-onset neurodevelopmental phenotype leading to death at ~12 weeks (Chen et al., 2001; Guy et al., 2001). This link between MeCP2 and a neurological disorder suggests that brain expression is of key functional importance. Accordingly, brain-specific depletion of MeCP2 produced mice that are indistinguishable from *Mecp2* null animals (Chen et al., 2001; Guy et al., 2001). Furthermore, a mouse model expressing MeCP2 under the *Tau* promoter, which is primarily neuron-specific, rescued the null animals (Luikenhuis et al., 2004). These observations highlight the importance of MeCP2 function in neurons.

Transfection experiments showed that MeCP2, when recruited to a promoter via a GAL4-binding domain, could repress transcription and that this repression was in part mediated by an interaction with histone deacetylase (HDAC)-containing complexes (Nan et al., 1998). These findings suggested that MeCP2 is a transcriptional repressor targeted to specific genes via DNA methylation. While subsequent studies have identified reproducible gene expression changes between wild-type and *Mecp2* null mouse brains, these are generally rather subtle (Jordan et al., 2007; Nuber et al., 2005), questioning the view that MeCP2 acts as a classical transcriptional repressor. In contrast to the original model, recent studies have proposed that MeCP2 modulates alternative splicing (Young et al., 2005) and acts as a transcriptional activator by recruiting the transcription factor CREB to specific genes (Chahrour et al., 2008). In addition, there have been reports that MeCP2 binding to DNA may not depend on methylation, as studies using in vitro chromatin assembly suggested that MeCP2 can bind to both methylated and nonmethylated DNA and mediate nucleosomal compaction (Georgel et al., 2003; Nikitina et al., 2007). Support for this view has come from chromatin immunoprecipitation-microarray (ChIP-chip) experiments using a neuronal cultured cell line. The report claimed that MeCP2 does not selectively bind methylated promoters, but instead is bound at many unmethylated promoters and has a similar binding pattern to RNA

polymerase II (Yasui et al., 2007). These findings call for a re-evaluation of the conventional view that MeCP2 recruits HDACs to methylated sites.

To distinguish these alternative hypotheses for MeCP2 function, we measured its abundance and distribution in the mature mouse brain. An additional motivation was to explain why MeCP2 abundance is so critical for its function. For example, expression of MeCP2 from transgenes in mice only brings about phenotypic rescue if the level of protein is close to that in wild-type brain; overexpression by ~2-fold is severely detrimental (Collins et al., 2004; Luikenhuis et al., 2004). These findings are mirrored in humans, where *MECP2* gene duplication events give rise to developmental delay and mental retardation (Lubs et al., 1999). We developed a technique to purify neuronal nuclei from the mature mouse brain and found that the absolute abundance of MeCP2 approaches the number of nucleosomes and methyl-CpG (meCpG) moieties in a diploid genome. Consistent with its high abundance, ChIP analysis showed MeCP2 to be globally distributed and to track the density of meCpG in the genome. Bisulfite sequencing of the immunoprecipitated DNA confirmed highly selective binding to methylated DNA sequences. In the absence of MeCP2, histone H3 acetylation (H3Ac) levels were globally elevated and histone H1 levels were doubled, suggesting that MeCP2 alters the global chromatin state. These changes were not seen in glia or other tissues where MeCP2 is much less abundant. We propose that a key neuron-specific role of MeCP2 is to impact the entire genome, rather than to act as a gene-specific regulator.

RESULTS

MeCP2 Is Enriched in Neuronal Nuclei and Almost as Abundant as Nucleosomes

As the correct expression level seems to be crucial to MeCP2 function (Collins et al., 2004; Guy et al., 2001; Luikenhuis et al., 2004), we wanted to determine the absolute abundance of MeCP2 in the mature brain. We first asked when during postnatal development MeCP2 reaches its maximum level by quantitative western blotting using mice of different ages (Figure S1A). MeCP2 was weakly detectable in neonatal brain, but increased rapidly to reach a maximum at ~5 weeks of age, after which total levels remained constant. We decided to use 6- to 8-week-old mice for all subsequent experiments. Immunofluorescence data have indicated that MeCP2 is predominantly expressed in neuronal nuclei, with much less being seen in glia (Kishi and Macklis, 2004). In order to focus on neurons, a procedure was developed to sort neuronal from glial nuclei using fluorescence-activated cell sorting (FACS). The vast majority of neuronal nuclei are positive for staining by the neuronal nuclear marker NeuN, whereas glial nuclei are negative (Mullen et al., 1992). NeuN staining of total brain nuclei gave a bimodal intensity distribution comprising 50% NeuN-positive nuclei (neurons) and 50% negative nuclei (predominantly glia) (Figure 1A). Staining of brain nuclei for MeCP2 gave a similar bimodal distribution: 56% high and 44% low MeCP2 staining (Figure 1B), with an approximately 6-fold difference in staining intensity. Sorting of nuclei on the basis of the NeuN staining purified a neuronal population and a predominantly glial population of nuclei (Figure 1C). As expected, NeuN-positive nuclei cosorted with the high MeCP2-expressing nuclei.

Quantitative western blotting using infrared imaging confirmed that both NeuN and MeCP2 levels were increased in the neuronal population and depleted in the predominantly glial population relative to unsorted brain nuclei (Figure 1D). We detected approximately 7-fold more MeCP2 in NeuN-positive versus NeuN-negative populations, similar to the difference in the staining intensities recorded by FACS (about 6-fold). Quantification of recombinant MeCP2 against a BSA standard (Figure S1B) allowed us to determine the absolute abundance of MeCP2 in unsorted nuclei isolated from mature mouse brain as 6×10^6 molecules per nucleus (Figures 1E and S1C). This result was verified using an independent MeCP2 antibody (Figure S1D). The amount of MeCP2 in sorted neuronal nuclei (NeuN-positive) was 16×10^6 molecules per nucleus, compared with $\sim 2 \times 10^6$ molecules per nucleus in the predominantly glial nuclear fraction (Figure 1F). For comparison, the abundance of MeCP2 in liver nuclei was 0.5×10^6 molecules per nucleus (Figure S1E). FACS staining suggested there may be some heterogeneity within the populations, indicating that these average values may not apply to each cell, as previously suggested (LaSalle et al., 2001). To relate MeCP2 levels to the core components of chromatin, we determined the abundance of histone H4 as 64×10^6 molecules per brain nucleus (Figure S1F), which corresponds to 32×10^6 nucleosomes in total, or one nucleosome per 165 bp of genomic DNA. The estimated number of meCpGs per diploid nucleus is 40×10^6 methylated CpG sites. Therefore, the number of MeCP2 molecules in the nucleus of a mature neuron approaches the number of histone octamers and meCpG sites and may be sufficient to almost "saturate" the genome.

MeCP2 Binds Globally across the Genome in the Mouse Brain

Previous reports using cultured neurons from embryonic or immature mice have suggested that MeCP2 binds at discrete genomic sites, such as at the brain-derived neurotrophic factor gene locus (*Bdnf*) (Chen et al., 2003) and at the *Dlx5/6* locus (Horike et al., 2005). As MeCP2 levels are low in immature mouse brain compared to the high abundance later on (Figure S1), the MeCP2 binding pattern in mature mice was determined. We used whole brain nuclei for MeCP2 ChIP as approximately ~89% of brain MeCP2 is derived from neuronal nuclei. We first tested the specificity of the 674 MeCP2 antibody (Nan et al., 1998) using the 234 bp mouse major satellite repeat, a known MeCP2 binding sequence, as a ChIP probe (Nan et al., 1996). Despite the MeCP2 antibody displaying relatively low efficiency (1.7% IP/Input), it was highly specific, exhibiting a 130-fold enrichment in wild-type compared to *Mecp2* null mouse brain (Figure 2A). We concluded that this degree of specificity was sufficient for analysis of MeCP2 binding in the genome.

Initially, we examined binding to the mouse *Bdnf* locus, which has eight alternative first exons, most of which are located in two large CGIs, with a large intervening intron. A panel of 22 ChIP primers was designed across a 39 kb region spanning the CGIs, and the MeCP2 binding profile was determined in mature mouse brain using ChIP and quantitative PCR. We observed significant enrichment across the entire region compared with

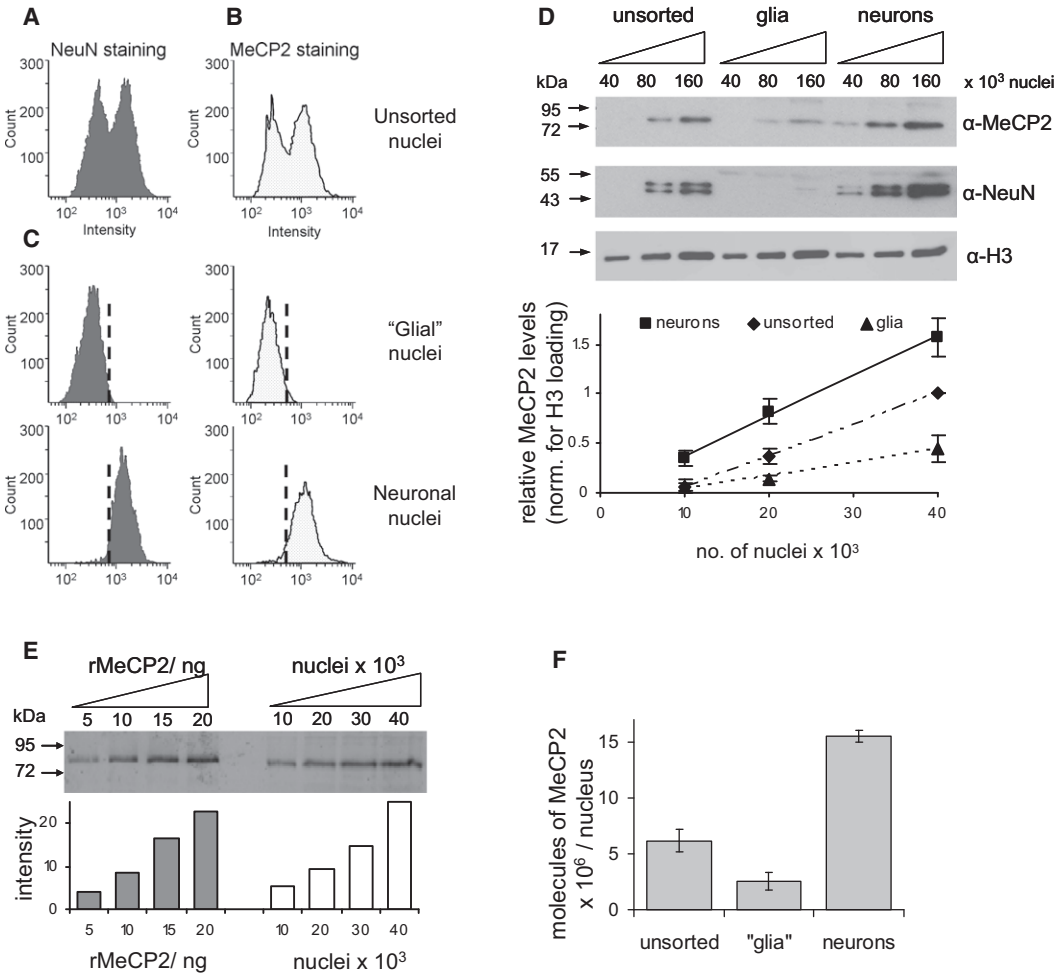

Figure 1. The Abundance of MeCP2 in Purified Neuronal Nuclei Approaches that of the Histone Octamer

(A and B) Nuclei were isolated from wild-type whole mouse brain and then FACS-stained for NeuN (A) and MeCP2 (B).

(C) Nuclei sorted for NeuN-negative and NeuN-positive staining cosorted with low-MeCP2- and high-MeCP2-stained nuclei, respectively.

(D) Infrared western blotting for NeuN, MeCP2, and histone H3 was performed on unsorted and FACS-sorted nuclei. The graph indicates quantification of western signals normalized for H3 loading.

(E) The level of MeCP2 in unsorted brain nuclei was quantified against recombinant MeCP2 by infrared western blotting (E). The graph below indicates densitometric analysis using LI-COR Odyssey.

(F) Densitometric analysis of western blots to determine absolute abundance of MeCP2 in the different nuclei populations. The positions of molecular weight markers (kDa) are indicated. Error bars indicate the mean ±SEM. See also Figure S1.

the *Mecp2* null brain, suggesting that MeCP2 is broadly distributed at the locus (Figure 2B). Interestingly, MeCP2 binding over the *Bdnf* CGIs is reduced relative to the surrounding regions, raising the possibility that these active promoters fail to attract MeCP2 due to their lack of DNA methylation. The intervening regions are CpG deficient by comparison with CGIs, but limited bisulfite DNA sequencing confirmed that they are largely methylated (data not shown). MeCP2 ChIP over the same region in wild-type liver gave a profile indistinguishable from the *Mecp2* null brain, suggesting this profile is a result of the high abundance in neurons. It was possible that the MeCP2 binding pattern in the whole brain is an aggregate of a large number of distinct patterns from individual regions and neuronal subtypes. To address this, the ChIP was repeated using a specific brain region: the hippocampus, which represents a relatively restricted subset of neuronal subtypes. The resulting MeCP2 binding profile was very similar to that of the wild-type whole brain, with MeCP2 bound over the entire locus but reduced over the CGIs (Figure 2B). This finding makes it likely that the ChIP results represent a consistent pattern across many types of neuron.

A similar approach was used to look at the MeCP2 binding across a 40 kb region encompassing the *Dlx5/6* locus. ChIP using mature mouse brain gave a reproducibly different pattern from that previously reported in neonatal mice by Horike et al., 2005, with MeCP2 bound across the entire region (Figure 2C). ChIP signal over the same region in *Mecp2* null brain was minimal, verifying the significance of the data. We next chose to examine MeCP2 occupancy over two housekeeping genes,

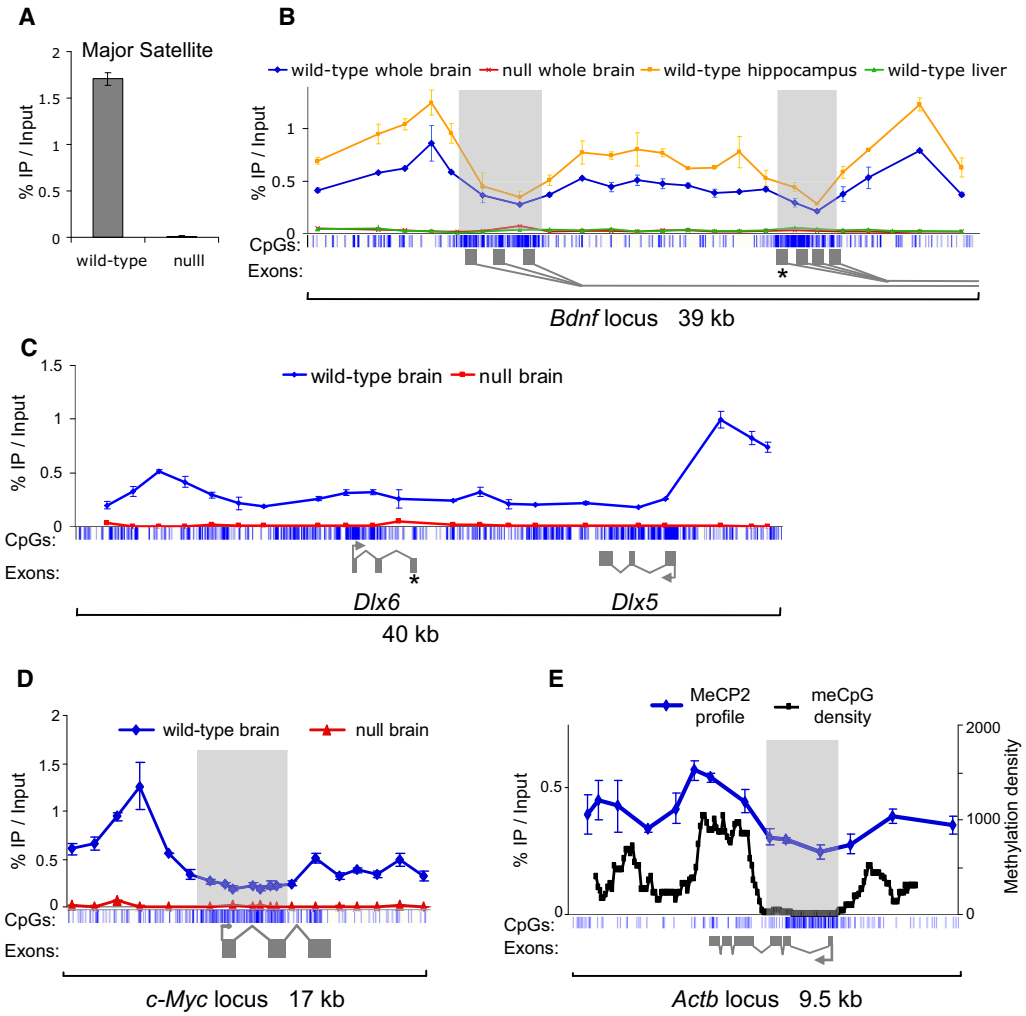

Figure 2. MeCP2 Shows Widespread Binding across Gene Loci in Mature Brain

(A) Mouse tissues (brain, hippocampus, and liver) were dissected, and ChIP was performed using an antibody against MeCP2. Immunoprecipitated DNA was analyzed by real-time PCR using a panel of primers. ChIP of the major satellite repeat shows 130-fold enrichment in wild-type brain compared to *Mecp2* null brain, indicating that the antibody is highly specific.

(B) MeCP2 binding profile across 39 kb of the promoter region of *Bdnf*. The blue vertical lines below the graph indicate CpG sites, with CGIs shaded in light gray. Alternative *Bdnf* exons 1 are indicated with dark gray rectangles. The asterisk marks the discrete binding site identified using cultured embryonic cortical neurons (Chen et al., 2003). ChIP was performed on various tissues as indicated.

(C) MeCP2 ChIP profile across a 40 kb region encompassing the *Dlx5/6* locus. The asterisk marks the key site identified using brains of 1-day-old mice. Wild-type whole brain is shown in blue and *Mecp2* null whole brain is shown in red.

(D) MeCP2 binding profile across the *c-Myc* locus in wild-type (blue) and *Mecp2* null (red) brains.

(E) MeCP2 binding profile across the *Actb* locus follows the meCpG density. MeCP2 ChIP was performed on wild-type brain (blue). Total brain genomic DNA was subjected to bisulfite sequencing for a continuous run of 262 CpG sites across ~9 kb. The methylation density is plotted based on a window size of 650 bp and step of 50 bp (shown in black). Error bars indicate mean ± SEM.

c-Myc and *Actb*, which have unmethylated CGIs flanked by methylated DNA that is comparatively CpG deficient. ChIP across the *c-Myc* locus showed MeCP2 bound to the methylated regions flanking the CGI, but as in the case of *Bdnf*, MeCP2 binding was depleted across the CGI (Figure 2D). Analysis of 9.5 kb surrounding the *Actb* locus showed a similar pattern with higher MeCP2 occupancy across the flanks, but depleted binding over the CGI (Figure 2E). In order to relate this result to meCpG density, we performed bisulfite sequencing to unambiguously determine modification of all 262 CpG sites across the *Actb* region (Figure 2E). The results confirm that the CGI is DNA methylation free, whereas the flanking region is predominantly methylated. Due to the variable CpG density, the methylation level varies dramatically across the locus. Significantly, the MeCP2 binding profile mirrors the methylation density through the region. Taken together, the results of these ChIP experiments fit with the hypothesis that MeCP2 binding tracks meCpG density.

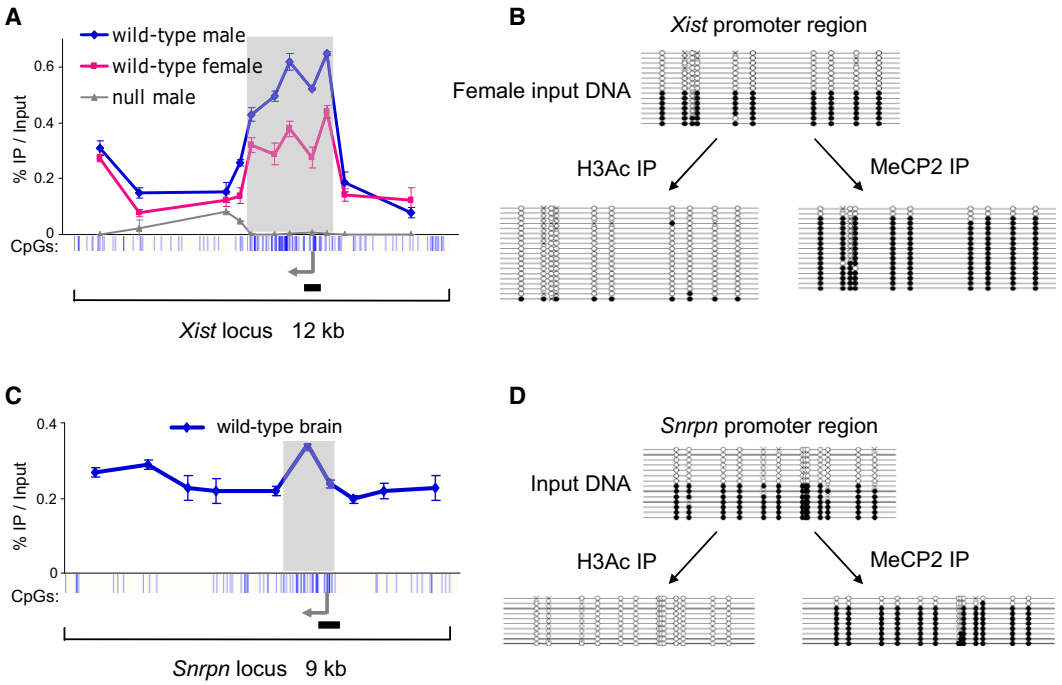

Figure 3. Brain MeCP2 Binds Selectively to Methylated DNA In Vivo

(A) Whole mouse brains were dissected, and ChIP was performed using antibodies against MeCP2 and acetylated histone H3. Input DNA and immunoprecipitated DNA were analyzed by real-time PCR and subjected to bisulfite sequencing. MeCP2 binding profiles across 12 kb of the *Xist* locus in wild-type male brain (blue), wild-type female brain (pink), and *Mecp2* null brain (gray) are shown in (A). The blue vertical lines below the graph indicate CpG sites, with the CGI shaded in light gray. The transcription start site is indicated with an arrow. The horizontal black line marks the region amplified for bisulfite sequencing.

(B) ChIP was performed on the wild-type female brain for MeCP2 and histone H3 acetylation. Recovered DNA was used for bisulfite sequencing of a region of the *Xist* promoter. Each line represents a single clone. Open and filled circles indicate nonmethylated and methylated CpG sites, respectively. Crosses indicate uncharacterized CpG sites.

(C) MeCP2 ChIP profile across 9 kb of the imprinted *Snrpn* locus in wild-type brain.

(D) ChIP was performed on the wild-type brain for MeCP2 and histone H3 acetylation. The resulting DNA was used for bisulfite sequencing of a region of the *Snrpn* promoter. Error bars indicate mean ±SEM.

MeCP2 Tracks the meCpG Density of the Genome

In the light of its high abundance and potentially global binding, we tested whether MeCP2 acts as a meCpG binding protein in neurons, or whether it interacts with chromatin regardless of DNA methylation, as proposed by in vitro chromatin assembly experiments (Georgel et al., 2003; Nikitina et al., 2007). We selected genomic regions that occur in both methylated and nonmethylated states within each cell and asked which of the two forms bound to MeCP2. First, we characterized binding over 12 kb of the X-linked *Xist* locus, comparing male to female mouse brains (Figure 3A). In male mice, there is a single methylated copy of the *Xist* promoter CGI, whereas in females there are two copies, one methylated and one nonmethylated (Hendrich et al., 1993). In the male brain, MeCP2 occupies the entire region, peaking over the densely methylated CGI. The finding that MeCP2 occupancy drops over nonmethylated CGIs (Figure 2) but peaks over methylated CGIs implies that MeCP2 is tracking the density of meCpG.

In females, MeCP2 occupancy flanking the *Xist* CGI is indistinguishable from the male profile. Over the *Xist* CGI, however, MeCP2 binding is reduced by half relative to the male brain (Figure 3A). This result is consistent with the notion that MeCP2 is only bound to one of the two *Xist* CGI alleles in the female. To test this more rigorously, we combined the ChIP protocol with bisulfite sequencing to determine the methylation status of the immunoprecipitated DNA. Input DNA from female brain gave approximately equal numbers of nonmethylated and methylated clones, as expected, confirming unbiased PCR amplification (Figure 3B). As a control, we bisulfite sequenced *Xist* DNA immunoprecipitated by an antibody against acetylated histone H3. This histone mark is specific for the active *Xist* allele and duly recovered the nonmethylated allele in 97% of clones (n = 39 clones). Following ChIP with anti-MeCP2 antibody, however, 88% of the recovered clones were methylated (n = 58 clones). A similar result was obtained by analyzing 9 kb of the imprinted *Snrpn* locus, which has a paternal unmethylated allele and a maternal methylated allele (Sutcliffe et al., 1994). MeCP2 is bound through the entire region, peaking over the imprinted CGI (Figure 3C). Using the ChIP-bisulfite protocol, the input DNA gave approximately equal numbers of nonmethylated and methylated clones (Figure 3D). As before, acetylated histone H3 ChIP recovered 100% nonmethylated clones (n = 23), whereas 89% of the clones obtained by MeCP2 ChIP were methylated (n = 19).

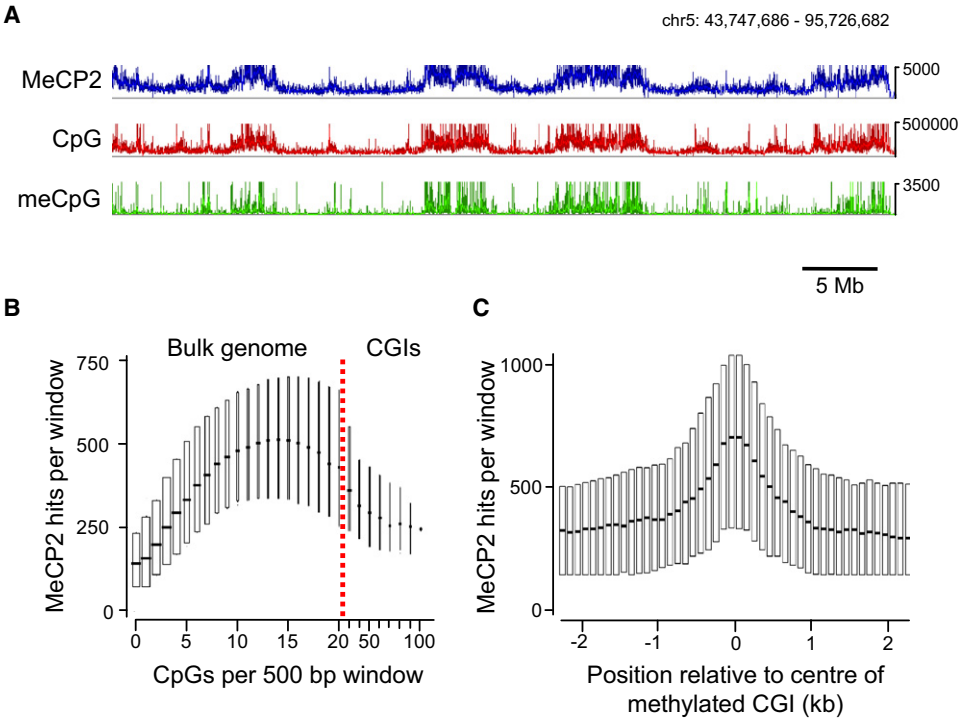

Figure 4. High-Throughput Sequencing of Immunoprecipitated Chromatin Shows MeCP2 Globally Distributed and Tracking the meCpG Density

(A) Profiles of MeCP2-bound sequences (blue), CpG density (red), and parallel sequencing from methyl-CpG (meCpG)-rich sequences (green) were analyzed using a sliding window (5 kb window; 1 kb step). A 52 Mb region of chromosome 5 is shown. The vertical axis represents sequencing hits or number of CpGs per window.

(B) The genome was scanned using a 500 bp window (100 bp step) and the number of MeCP2 hits per window plotted against the number of CpGs per window. Box plots are shown with the horizontal line indicating the median and the surrounding box showing the interquartile range. The width of the box is proportional to the fraction of the genome that corresponds with that CpG density. The majority of CGIs contain greater than 5 CpG sites/100 bp as indicated by red line, whereas the bulk genome has a lower CpG density.

(C) Methylated CGIs were identified by meCpG affinity chromatography. The surrounding 5 kb of genomic DNA was analyzed for MeCP2 binding using a 500 bp window (100 bp step). Results are presented as for (B). See Figure S2.

We conclude that MeCP2 preferentially binds to the methylated allele in each case.

High-Throughput Sequencing Confirms Genome-wide Binding

Analysis of candidate loci across ~150 kb of the mouse brain genome suggests that MeCP2 is widely distributed. To view MeCP2 occupancy genome-wide, we performed high-throughput DNA sequencing of total MeCP2-bound chromatin. In all, 2.9×10^9 bases were sequenced, of which 1.3×10^9 were uniquely mappable. Despite relatively extensive sequencing, clear peaks were not identified. Instead, sequencing reads were dispersed throughout the genome, covering 56% of the mouse genome (2.5×10^9 bp, of which 1.8×10^9 is repeat masked). This result fits with our analysis of candidate regions by ChIP-PCR. Since MeCP2 binding is genome-wide, it would be necessary to sequence the entire genome several-fold to obtain a comprehensive high-resolution profile. With 56% genome coverage, however, we were able to robustly test for a relationship with DNA methylation by comparing the profile of the CpG sequence in a sliding 5 kb window with that of MeCP2. The match was striking (Figure 4A), suggesting that MeCP2 binding coincides with this dinucleotide sequence, which is ~70% methylated in brain DNA (Ehrlich et al., 1982). As a more direct test, we determined the distribution of meCpG by fractionating whole genomic DNA based on its affinity for an immobilized meCpG-binding domain (Cross et al., 1994; Illingworth et al., 2008). Retained sequences were analyzed by high-throughput sequencing. An earlier comparison between this method of meCpG mapping and use of an anti-meC antibody (MeDIP) indicated that both are equally effective at measuring meCpG density (Zhang et al., 2006). We conclude that in vivo-bound MeCP2 mirrors meCpG over long regions of chromosomal DNA (Figure 4A).

In a second test for the relationship between MeCP2 binding and meCpG, we asked whether the depression of MeCP2 binding seen at nonmethylated CGIs associated with the *c-Myc*, *Dlx5/6*, *Actb*, and *Bdnf* loci applied genome-wide. We binned the mouse genome sequence according to CpG density in 500 bp windows and determined the level of MeCP2 binding in each bin. The results (Figure 4B) show that MeCP2 binding initially increases with base composition, as predicted by

Figure 4A, but drops steeply at densities above 25 CpGs per 500 bp. This density predominantly reflects nonmethylated CGIs (Figure S2). Third, we examined the binding of MeCP2 to methylated CGIs, as analysis of the *Xist* and *Snrpn* loci suggested increased binding (Figure 3). The results show a peak of MeCP2 binding centered over methylated CGIs (Figure 4C). These findings match closely the predictions based on candidate regions of the genome (Figure 2) and therefore reinforce the conclusion that MeCP2 tracks DNA methylation genome-wide.

MeCP2 Globally Alters the Chromatin State

The high abundance of MeCP2 in neurons suggests that it may influence chromatin structure globally. It was previously reported that in the *Mecp2* mutant mouse brain, levels of histone H3Ac are elevated (Shahbazian et al., 2002). As approximately 89% of MeCP2 is in the neurons, we hypothesized that any differences in chromatin state between wild-type and *Mecp2* null brain would be restricted to the neurons but be absent from glia. To test this, we compared H3Ac levels in unsorted nuclei with purified neuronal and glial nuclei by western blotting (Figure 5A). Unsorted *Mecp2* null brain nuclei displayed a 1.5-fold increase in H3Ac compared to wild-type. This difference increased significantly to 2.6-fold in sorted neuronal nuclei (Kolmogorov-Smirnov [KS] test $p \leq 0.01$), whereas glial nuclei consistently showed no significant increase in H3Ac (0.9-fold decrease). We conclude that the small elevation of H3Ac seen in whole brain is entirely due to neurons where MeCP2 is highly abundant. Our findings do not corroborate a recent report that histone H3Ac is increased in *Mecp2* null glia (Ballas et al., 2009).

Widespread chromosome binding by MeCP2 might be expected to modulate chromatin structure globally rather than at specific sites. We asked whether ChIP using an anti-acetyl H3 antibody could detect alterations across specific chromatin domains in the MeCP2-deficient brain. Due to low recovery of neuronal nuclei via FACS, whole brain was used, although this probably leads to an underestimate of changes in neuronal chromatin. Across the 39 kb *Bdnf* region, H3Ac peaked over the active promoter CGI regions in both wild-type and null (Figure 5B), but was low in flanking regions. Comparing wild-type and mutant brain, levels of immunoprecipitated DNA in the mutant were elevated by 2-fold relative to input throughout the region (KS test $p < 0.004$). Interestingly, the magnitude of the effect mirrored the pattern of MeCP2 binding (Figure 5B), being lowest where MeCP2 binds least (the CGIs) and highest where most MeCP2 is relatively concentrated. This is compatible with a simple causal relationship between binding of MeCP2 and levels of histone deacetylation. A 1.4-fold elevation in histone acetylation was also seen in regions of the male *Xist* locus flanking the CGI (Figure S3) (KS test $p = 0.03$). This difference was notably absent over the *Xist* CGI itself, implying that repression of histone acetylation at this DNA promoter sequence is not solely dependent on MeCP2. Altogether, we examined 100 loci covering 90 kb of genomic DNA by quantitative PCR and found an average 1.4-fold elevation in H3Ac (KS test $p < 0.002$). These data indicate that the global chromosomal association of MeCP2 imposes a reduction in histone acetylation levels across the genome (Figure 5C).

Histone H1 is present in most cell types at an approximate stoichiometry of one molecule per nucleosome (Woodcock et al., 2006), but uniquely, in neurons, this is reduced to one molecule every two nucleosomes (Allan et al., 1984; Pearson et al., 1984). Chromatin reconstitution experiments showed that MeCP2 can compete with histone H1 for binding to methylated chromatin and may function as a substitute linker histone (Ishibashi et al., 2008; Nan et al., 1997). As MeCP2 occurs at approximately one molecule per two nucleosomes in neurons, we asked whether the abundance of histone H1 was affected by MeCP2 depletion. Using FACS-purified neuronal nuclei, we found that histone H1 is elevated ~2-fold in the *Mecp2* null compared to the wild-type (Figure 5D) (KS test $p < 0.05$). No difference was seen in unsorted nuclei from wild-type and mutant whole brain, suggesting that this effect is specific to neurons where MeCP2 is highly abundant. The level of histone H1 present in MeCP2-deficient neurons appears to be close to one molecule per nucleosome, as seen in other cell types, suggesting that the reduced level in neurons may reflect substitution of H1 by MeCP2.

MeCP2 Suppresses Spurious Transcription of Repetitive Elements

Our results implicate MeCP2 as a global regulator of neuronal chromatin structure. A possible outcome of MeCP2 depletion is that increased histone acetylation could lead to inappropriate transcription from the bulk genome, including dispersed repetitive elements. To test this possibility, we studied expression of L1 retrotransposons, intracisternal A particles, and tandem repetitive units of the mouse major satellite, which are methylated and bound by MeCP2 (Figure S4A). RNA was extracted from the whole brain, and RT-PCR was used to determine the expression levels of these elements. No difference was observed between wild-type and *Mecp2* null brain (Figure S4B). We considered, however, that spurious transcripts might be degraded by the exosome and therefore not survive as stable components of cytoplasmic RNA. To reduce the opportunities for transcript degradation, RNA was extracted from isolated nuclei and analyzed by RT-PCR. The same repetitive regions now showed significantly increased levels of expression in the *Mecp2* null brain compared to the wild-type (Figure 6A). In contrast, no differences in the expression levels of *Actb*, *c-Myc*, or *tyrosine hydroxylase* mRNAs were observed (Figure 6A). On average, repetitive regions showed 1.6-fold overexpression in the *Mecp2* null brain (four biological replicates; KS test $p < 0.0002$), whereas the expression of these bona fide genes was unaffected (Figures 6B and S4D). These results do not preclude the possibility that some genes show changes in the *Mecp2* null brain. They argue, however, that one consequence of MeCP2-deficiency in neurons is an increase in transcriptional noise. This effect was not seen in embryonic brains from E18.5 mice (Figure S4C), suggesting that increased transcriptional noise is confined to the mature brain where MeCP2 is abundant enough to impact the whole genome.

DISCUSSION

Mouse models and human neurological disorders suggest that appropriate levels of MeCP2 are essential for its proper function,

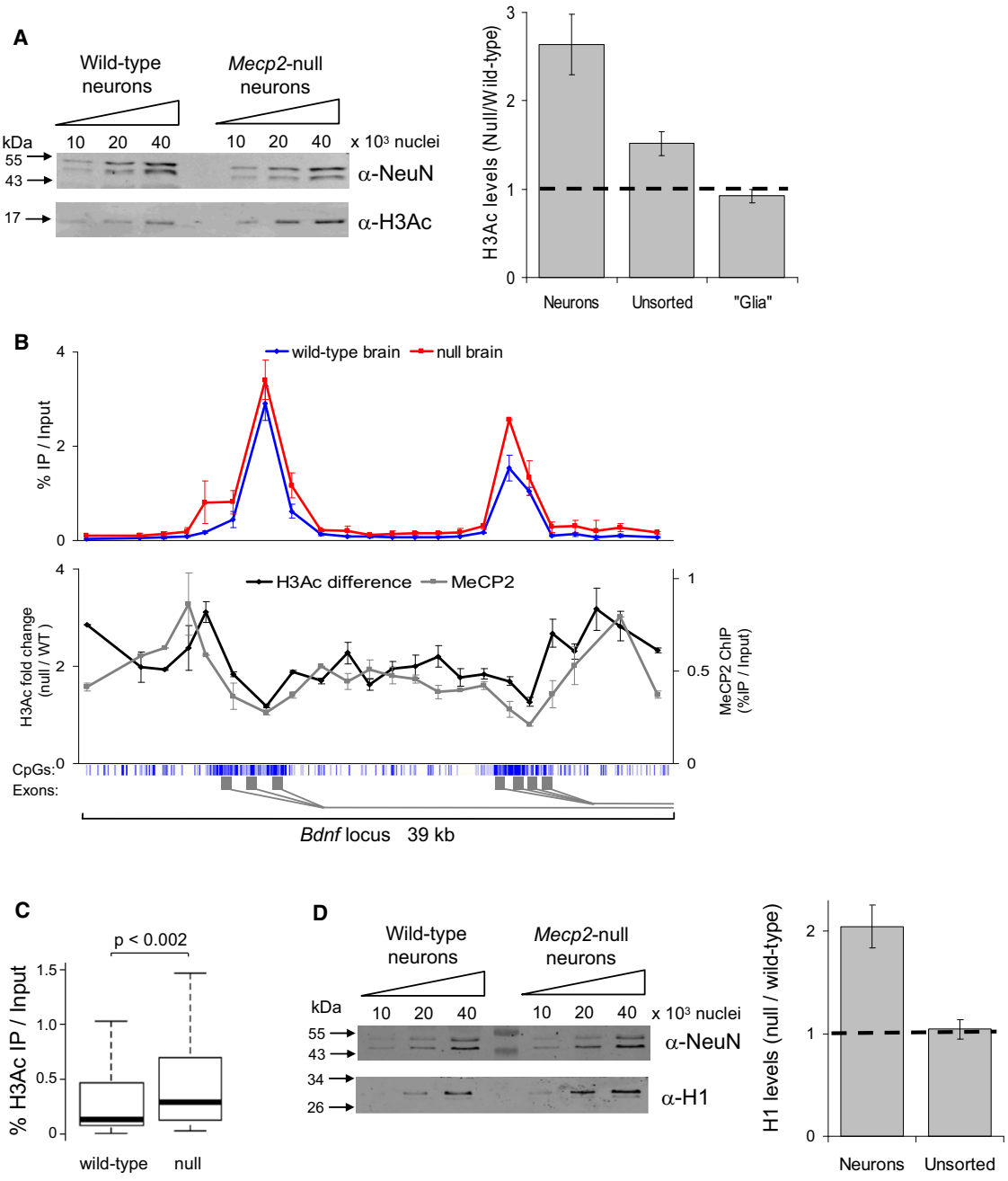

Figure 5. MeCP2 Deficiency Affects the Global Chromatin State by Elevating Levels of Histone H3 Acetylation (H3Ac) and the Linker Histone H1

(A) H3Ac levels were determined by quantitative western blotting of unsorted brain nuclei and FACS-purified nuclei from both wild-type and *Mecp2* null brain. The western blot shows H3Ac levels and NeuN (as a loading control) in the purified neuronal nuclei. The graph indicates densitometric analysis of H3Ac levels in the different nuclei populations, normalized for differences in loading. The horizontal line represents no change between wild-type and *Mecp2* null.

(B) The upper graph shows the H3Ac profile across the promoter region of the *Bdnf* locus in wild-type (blue) and *Mecp2* null (red) brains. The lower graph indicates the H3Ac fold difference between wild-type and *Mecp2* null brain (grey); the MeCP2 ChIP profile is also shown (black). The blue vertical lines below the graph indicate CpG sites, with the CGI shaded in light gray. The gene structure is indicated by dark gray rectangles below. These data represent the average of three independent experiments.

(C) Box plot showing all H3Ac ChIP results for wild-type and *Mecp2* null brain (n = 100).

(D) Quantitative western blotting for histone H1 and NeuN (as a loading control) using FACS-purified neuronal nuclei from wild-type and *Mecp2* null mice. The graph indicates densitometric analysis of H1 levels in the different nuclei populations. Error bars indicate mean ±SEM, and the KS test was used to determine statistical significance. See also Figure S3.

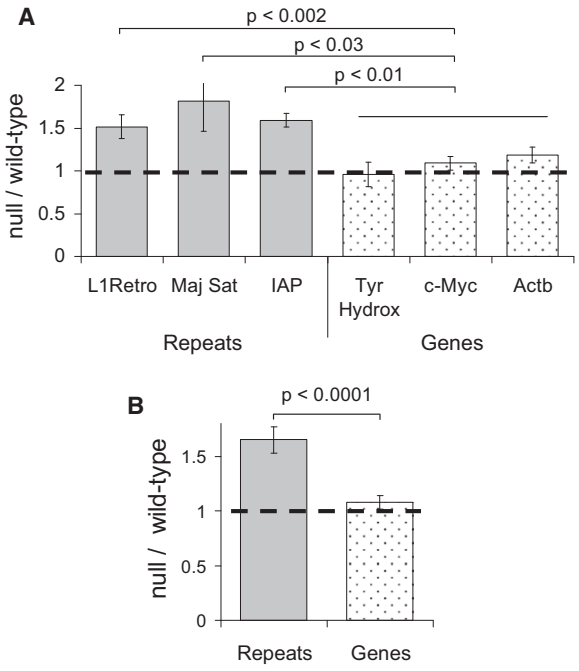

Figure 6. MeCP2 Suppresses Transcription from Repetitive Elements Distributed Throughout the Genome

(A) Nuclei were isolated from wild-type and *Mecp2* null brains. RNA was extracted and cDNA was prepared with and without reverse transcriptase. Quantitative PCR was used to determine the expression levels of repetitive regions and genic regions. The data were normalized to GAPDH and shown as a ratio between *Mecp2* null and wild-type nuclei. The horizontal line represents no change between wild-type and *Mecp2* null mice.

(B) Shows the pooled data, grouping repetitive regions and genic regions. Error bars indicate mean ±SEM. The KS test was used to determine statistical significance. See Figure S4.

as both deficiency and mild overexpression result in a neurological phenotype (Collins et al., 2004; Guy et al., 2001). Our data establish MeCP2 as one of the most abundant nuclear proteins in mature neurons. With an average density of one molecule every two nucleosomes, there is enough to bind approximately half of all meCpG sites in the diploid neuronal genome. ChIP analysis of candidate regions and high-throughput sequencing confirm that MeCP2 is globally bound and tracks the density of meCpG in the genome. As for all ChIP analyses, it is possible that there are transient interactions that are not captured using formaldehyde crosslinking (Schmiedeberg et al., 2009), and we may therefore be selectively visualizing stable MeCP2-DNA interactions.

Our evidence supports earlier contentions that the large number of potential binding sites fits with a global regulatory role (Nan et al., 1997). Although provisional identification of MeCP2 "target genes" has been supported by MeCP2-ChIP near specific promoters, it is now apparent that most regions of the genome, including repetitive sequences and intergenic DNA, are associated with MeCP2 in neurons. The notion that MeCP2 resembles a transcription factor by being targeted to a specific subset of genes appears to be incorrect.

In line with its high abundance, MeCP2 impacts the chromatin state globally. Histone H1 is atypically low in neurons, being sufficient only to bind half of all neuronal nucleosomes, whereas in other cell types the stoichiometry is almost one-to-one (Allan et al., 1984; Pearson et al., 1984). We found that when MeCP2 is absent, the amount of neuronal H1 doubles, bringing it to the level typical of most cell types. There was no comparable effect in glia, where the density of chromosome-bound MeCP2 is much lower. MeCP2 can compete with H1 for binding to chromatin containing methylated DNA in vitro (Nan et al., 1997). Further in vitro studies have suggested that MeCP2 may function in a manner analogous to a linker histone, as it can bind to entry-exit sites on nucleosomes and promote the formation of higher order structures (Ishibashi et al., 2008; Nikitina et al., 2007). It is tempting to propose that competition for chromatin binding sites between neuronal MeCP2 and H1 displaces the linker histone from half of its potential sites, leading to a reduction in the requirement for H1. In the *Mecp2* null brain, where this competition does not occur, H1 is apparently restored to its conventional nucleosomal stoichiometry of 1:1 and may functionally compensate in part for MeCP2 deficiency. Further work is needed to clarify the role of MeCP2 as a putative alternative linker histone.

Elevated histone acetylation in MeCP2-deficient whole-brain samples has been reported previously (Shahbazian et al., 2002). By sorting neuronal from glial nuclei, we show that this difference is entirely due to a large change in neurons, with no corresponding alteration detectable in glia. Using ChIP, we show that this increase is distributed throughout the genome rather than at distinct sites. Early evidence suggested that MeCP2 can recruit the HDAC-containing complexes (Nan et al., 1998). A plausible model, therefore, is that MeCP2 attracts corepressors throughout the genome, which depress histone acetylation according to the local density of meCpG. The finding that the ratio of mutant to wild-type H3Ac matches the density profile of MeCP2 (Figure 5B) provides support for this contention. We propose that these global effects of MeCP2 deficiency on both H1 abundance and histone acetylation are seen exclusively in neurons because only in these cells is MeCP2 sufficiently abundant to coat the genome. In other cell types, the low density of MeCP2 occupancy is insufficient to impact bulk chromatin.

Studies with in vitro reconstituted chromatin have suggested that MeCP2 might play a structural role in chromatin regardless of DNA methylation (Georgel et al., 2003). Against this hypothesis, other studies have showed MeCP2 preferentially binds methylated DNA (Gregory et al., 2001; Nan et al., 1996). We establish that even in neurons, where MeCP2 abundance is equivalent to that of histone H1, DNA methylation dependence still holds. These in vivo data reinforce the view that MeCP2 binding depends upon the methylation status of chromosomal DNA. This dependence may account for the remarkable reversibility of severe neurological symptoms in mice when MeCP2 is restored following development under MeCP2-deficient conditions (Guy et al., 2007). If, as seems likely, DNA methylation patterns are laid down normally in the absence of MeCP2, then the restored protein is expected to distribute

correctly according to these genomic cues and take up its usual function.

The global distribution of MeCP2 casts light on gene expression studies, which initially detected few significant changes between *Mecp2* null and wild-type brain (Jordan et al., 2007) but more recently have reported large numbers of subtle alterations comprising both increases and decreases in gene expression (Chahrour et al., 2008). Where a transcriptional regulator affects a restricted number of genes, coherent expression changes at those genes are expected when the protein is deficient. If, however, a large proportion of all genes are affected, it is more difficult to predict how deficiency will impact expression. The HDAC inhibitor trichostatin A, for example, causes dramatic hyperacetylation of histones, but despite the clear association between histone hyperacetylation and transcriptional activity, the drug usually causes equal numbers of genes to be up- and downregulated (Peart et al., 2005). A potential explanation is that the nucleus contains limiting supplies of transcriptional machinery, so that increased expression at some loci must be matched by decreases at others, even if all genes are potentially activated by hyperacetylation. By analogy, the high abundance of MeCP2 may mean that many genes are potentially affected, but analysis of stable gene expression patterns following long-term absence of MeCP2 may not accurately reflect these effects.

Our hypothesis that high levels of MeCP2 affect global chromatin structure is supported by elevated transcriptional noise from repetitive elements in nuclei of the *Mecp2* null brain. This effect is absent in embryonic brains, suggesting that the abundance of MeCP2 is key. Expression of bona fide genes, on the other hand, was not elevated, which may mean either that most transcription rates are little changed or that posttranscriptional controls are able to compensate. We suggest that globally bound MeCP2 dampens transcription in a genome-wide manner by recruiting HDAC activity and acting as a linker histone. Why might neurons have evolved a requirement for MeCP2 as a genome-wide transcriptional dampener, whereas other somatic tissues have not? One possibility is that the neurons are particularly sensitive to the levels of transcriptional noise from the bulk genome and therefore have a special need for MeCP2 to quench this. Another potential explanation is that neuronal plasticity and homeostasis depend upon the specific ability of MeCP2 to respond dynamically to activity. Neuronal firing leads to a burst of synaptic protein synthesis and nuclear transcription, which is required for development of synaptic systems (Bading, 2000). MeCP2 undergoes site-specific phosphorylation following synaptic firing, which is reported to alter its affinity for DNA and its nuclear distribution (Chen et al., 2003; Zhou et al., 2006). We speculate that phosphorylation may transiently relieve the genome-wide repressive chromatin structure maintained by MeCP2 and thereby facilitate appropriate gene expression. Further reports of posttranslational modifications of MeCP2 (Tao et al., 2009) raise the possibility that MeCP2 is a signaling hub within neurons and as such may play a crucial role in neuronal maintenance. Recognition of MeCP2 as a global chromatin regulator that is responsive to neuronal activity promises to shed light on the molecular basis of Rett syndrome.

EXPERIMENTAL PROCEDURES

Mouse Models

C57BL/6 Mecp2$^{tm1.1Bird}$ mice were used, with wild-type littermates as controls. Unless otherwise stated, all mice were 6–8 weeks of age. Mice were euthanized by CO_2 asphyxiation. Tissues were dissected and either frozen in nitrogen for ChIP or used directly for nuclear preparation.

Nuclei Preparation

Mouse brain nuclei were isolated as previously described (Klose and Bird, 2004). Recovered nuclei were resuspended in 1 × PBS supplemented with 20% glycerol, 10 mM sodium butyrate, and complete protease inhibitors (Roche; Indianapolis, IN); frozen in liquid nitrogen; and stored at −80°C. Serial dilutions of nuclei were counted using a hemocytometer to determine concentration. Nuclei were lysed in Laemmli buffer and used directly for gel electrophoresis.

Fluorescence-Activated Cell Sorting

Detailed protocols are available in the Supplemental Information.

Gel Electrophoresis and Western Blotting

Proteins were resolved by SDS-PAGE and transferred to PVDF membrane. Visualization of reactive proteins was performed by enhanced chemiluminescence and quantitative infrared imaging (LI-COR Odyssey, LI-COR Biosciences; Lincoln, NE). Intensity of protein bands was quantified using NIH ImageJ and LI-COR software. Details of recombinant proteins are in the Supplemental Information.

ChIP and Solexa Analysis

Detailed protocols are available in the Supplemental Information.

Bisulfite Sequencing

Bisulfite treatment of DNA and sequencing was carried out as previously described (Illingworth et al., 2008).

Expression Analysis

For whole-cell expression analysis, RNA was extracted using TriReagent (Sigma-Aldrich; St. Louis) from whole brain disrupted using a polytron (Janke and Kunkel; Wilmington, NC). For nuclear expression analysis, equal numbers of nuclei were lysed in extraction buffer (30 mM Tris-HCl [pH 7.5], 300 mM NaCl, 10 mM EDTA, 1% SDS, 0.5 mg/ml Proteinase K, 0.2 U/μl RNAsin) for 45 min at 37°C. Subsequently, the RNA was extracted using acid phenol and then precipitated with ethanol. After DNaseI treatment (Ambion DNA-free; Foster City, CA), cDNA was transcribed using Moloney murine leukemia virus reverse transcriptase (Promega; Madison, WI). Real-time PCR was carried out using Quantace SensiMix Plus (primer sequences are available on request).

ACCESSION NUMBERS

High-throughput sequencing data have been deposited in the Gene Expression Omnibus (GEO) under the accession number GSE19786.

SUPPLEMENTAL INFORMATION

Supplemental Information includes Supplemental Experimental Procedures and four figures and can be found with this article online at doi:10.1016/j.molcel.2010.01.030.

ACKNOWLEDGMENTS

We are grateful to Elizabeth Sheridan for testing the DNA sequencing protocol and to Stuart McLaren, Katherine Auger, and Julian Parkhill (Wellcome Trust Sanger Institute) for coordinating the DNA sequencing. We also thank Jim Selfridge, Jacky Guy, and Aimée Deaton for critical comments on the manuscript. This work was supported by the Wellcome Trust and by the "Epigenome" European Union Network of Excellence.

Received: August 13, 2009
Revised: November 17, 2009
Accepted: January 22, 2010
Published: February 25, 2010

REFERENCES

Allan, J., Rau, D.C., Harborne, N., and Gould, H. (1984). Higher order structure in a short repeat length chromatin. J. Cell Biol. *98*, 1320–1327.

Amir, R.E., Van den Veyver, I.B., Wan, M., Tran, C.Q., Francke, U., and Zoghbi, H.Y. (1999). Rett syndrome is caused by mutations in X-linked MECP2, encoding methyl-CpG-binding protein 2. Nat. Genet. *23*, 185–188.

Armstrong, D.D. (2002). Neuropathology of Rett syndrome. Ment. Retard. Dev. Disabil. Res. Rev. *8*, 72–76.

Bading, H. (2000). Transcription-dependent neuronal plasticity the nuclear calcium hypothesis. Eur. J. Biochem. *267*, 5280–5283.

Ballas, N., Lioy, D.T., Grunseich, C., and Mandel, G. (2009). Non-cell autonomous influence of MeCP2-deficient glia on neuronal dendritic morphology. Nat. Neurosci. *12*, 311–317.

Balmer, D., Goldstine, J., Rao, Y.M., and LaSalle, J.M. (2003). Elevated methyl-CpG-binding protein 2 expression is acquired during postnatal human brain development and is correlated with alternative polyadenylation. J. Mol. Med. *81*, 61–68.

Bird, A., Taggart, M., Frommer, M., Miller, O.J., and Macleod, D. (1985). A fraction of the mouse genome that is derived from islands of nonmethylated, CpG-rich DNA. Cell *40*, 91–99.

Chahrour, M., Jung, S.Y., Shaw, C., Zhou, X., Wong, S.T., Qin, J., and Zoghbi, H.Y. (2008). MeCP2, a key contributor to neurological disease, activates and represses transcription. Science *320*, 1224–1229.

Chen, R.Z., Akbarian, S., Tudor, M., and Jaenisch, R. (2001). Deficiency of methyl-CpG binding protein-2 in CNS neurons results in a Rett-like phenotype in mice. Nat. Genet. *27*, 327–331.

Chen, W.G., Chang, Q., Lin, Y., Meissner, A., West, A.E., Griffith, E.C., Jaenisch, R., and Greenberg, M.E. (2003). Derepression of BDNF transcription involves calcium-dependent phosphorylation of MeCP2. Science *302*, 885–889.

Collins, A.L., Levenson, J.M., Vilaythong, A.P., Richman, R., Armstrong, D.L., Noebels, J.L., David Sweatt, J., and Zoghbi, H.Y. (2004). Mild overexpression of MeCP2 causes a progressive neurological disorder in mice. Hum. Mol. Genet. *13*, 2679–2689.

Cross, S.H., Charlton, J.A., Nan, X., and Bird, A.P. (1994). Purification of CpG islands using a methylated DNA binding column. Nat. Genet. *6*, 236–244.

Ehrlich, M., Gama-Sosa, M.A., Huang, L.H., Midgett, R.M., Kuo, K.C., McCune, R.A., and Gehrke, C. (1982). Amount and distribution of 5-methylcytosine in human DNA from different types of tissues of cells. Nucleic Acids Res. *10*, 2709–2721.

Georgel, P.T., Horowitz-Scherer, R.A., Adkins, N., Woodcock, C.L., Wade, P.A., and Hansen, J.C. (2003). Chromatin compaction by human MeCP2. Assembly of novel secondary chromatin structures in the absence of DNA methylation. J. Biol. Chem. *278*, 32181–32188.

Gregory, R.I., Randall, T.E., Johnson, C.A., Khosla, S., Hatada, I., O'Neill, L.P., Turner, B.M., and Feil, R. (2001). DNA methylation is linked to deacetylation of histone H3, but not H4, on the imprinted genes Snrpn and U2af1-rs1. Mol. Cell. Biol. *21*, 5426–5436.

Guy, J., Hendrich, B., Holmes, M., Martin, J.E., and Bird, A. (2001). A mouse Mecp2-null mutation causes neurological symptoms that mimic Rett syndrome. Nat. Genet. *27*, 322–326.

Guy, J., Gan, J., Selfridge, J., Cobb, S., and Bird, A. (2007). Reversal of neurological defects in a mouse model of Rett syndrome. Science *315*, 1143–1147.

Hendrich, B.D., Brown, C.J., and Willard, H.F. (1993). Evolutionary conservation of possible functional domains of the human and murine XIST genes. Hum. Mol. Genet. *2*, 663–672.

Horike, S., Cai, S., Miyano, M., Cheng, J.F., and Kohwi-Shigematsu, T. (2005). Loss of silent-chromatin looping and impaired imprinting of DLX5 in Rett syndrome. Nat. Genet. *37*, 31–40.

Illingworth, R., Kerr, A., Desousa, D., Jørgensen, H., Ellis, P., Stalker, J., Jackson, D., Clee, C., Plumb, R., Rogers, J., et al. (2008). A novel CpG island set identifies tissue-specific methylation at developmental gene loci. PLoS Biol. *6*, e22.

Ishibashi, T., Thambirajah, A.A., and Ausió, J. (2008). MeCP2 preferentially binds to methylated linker DNA in the absence of the terminal tail of histone H3 and independently of histone acetylation. FEBS Lett. *582*, 1157–1162.

Jordan, C., Li, H.H., Kwan, H.C., and Francke, U. (2007). Cerebellar gene expression profiles of mouse models for Rett syndrome reveal novel MeCP2 targets. BMC Med. Genet. *8*, 36.

Kishi, N., and Macklis, J.D. (2004). MECP2 is progressively expressed in post-migratory neurons and is involved in neuronal maturation rather than cell fate decisions. Mol. Cell. Neurosci. *27*, 306–321.

Klose, R.J., and Bird, A.P. (2004). MeCP2 behaves as an elongated monomer that does not stably associate with the Sin3a chromatin remodeling complex. J. Biol. Chem. *279*, 46490–46496.

LaSalle, J.M., Goldstine, J., Balmer, D., and Greco, C.M. (2001). Quantitative localization of heterogeneous methyl-CpG-binding protein 2 (MeCP2) expression phenotypes in normal and Rett syndrome brain by laser scanning cytometry. Hum. Mol. Genet. *10*, 1729–1740.

Lewis, J.D., Meehan, R.R., Henzel, W.J., Maurer-Fogy, I., Jeppesen, P., Klein, F., and Bird, A. (1992). Purification, sequence, and cellular localization of a novel chromosomal protein that binds to methylated DNA. Cell *69*, 905–914.

Lubs, H., Abidi, F., Bier, J.A., Abuelo, D., Ouzts, L., Voeller, K., Fennell, E., Stevenson, R.E., Schwartz, C.E., and Arena, F. (1999). XLMR syndrome characterized by multiple respiratory infections, hypertelorism, severe CNS deterioration and early death localizes to distal Xq28. Am. J. Med. Genet. *85*, 243–248.

Luikenhuis, S., Giacometti, E., Beard, C.F., and Jaenisch, R. (2004). Expression of MeCP2 in postmitotic neurons rescues Rett syndrome in mice. Proc. Natl. Acad. Sci. USA *101*, 6033–6038.

Mullen, R.J., Buck, C.R., and Smith, A.M. (1992). NeuN, a neuronal specific nuclear protein in vertebrates. Development *116*, 201–211.

Nan, X., Tate, P., Li, E., and Bird, A. (1996). DNA methylation specifies chromosomal localization of MeCP2. Mol. Cell. Biol. *16*, 414–421.

Nan, X., Campoy, F.J., and Bird, A. (1997). MeCP2 is a transcriptional repressor with abundant binding sites in genomic chromatin. Cell *88*, 471–481.

Nan, X., Ng, H.H., Johnson, C.A., Laherty, C.D., Turner, B.M., Eisenman, R.N., and Bird, A. (1998). Transcriptional repression by the methyl-CpG-binding protein MeCP2 involves a histone deacetylase complex. Nature *393*, 386–389.

Nikitina, T., Shi, X., Ghosh, R.P., Horowitz-Scherer, R.A., Hansen, J.C., and Woodcock, C.L. (2007). Multiple modes of interaction between the methylated DNA binding protein MeCP2 and chromatin. Mol. Cell. Biol. *27*, 864–877.

Nuber, U.A., Kriaucionis, S., Roloff, T.C., Guy, J., Selfridge, J., Steinhoff, C., Schulz, R., Lipkowitz, B., Ropers, H.H., Holmes, M.C., and Bird, A. (2005). Up-regulation of glucocorticoid-regulated genes in a mouse model of Rett syndrome. Hum. Mol. Genet. *14*, 2247–2256.

Pearson, E.C., Bates, D.L., Prospero, T.D., and Thomas, J.O. (1984). Neuronal nuclei and glial nuclei from mammalian cerebral cortex. Nucleosome repeat lengths, DNA contents and H1 contents. Eur. J. Biochem. *144*, 353–360.

Peart, M.J., Smyth, G.K., van Laar, R.K., Bowtell, D.D., Richon, V.M., Marks, P.A., Holloway, A.J., and Johnstone, R.W. (2005). Identification and functional significance of genes regulated by structurally different histone deacetylase inhibitors. Proc. Natl. Acad. Sci. USA *102*, 3697–3702.

Schmiedeberg, L., Skene, P., Deaton, A., and Bird, A. (2009). A temporal threshold for formaldehyde crosslinking and fixation. PLoS ONE *4*, e4636.

Shahbazian, M., Young, J., Yuva-Paylor, L., Spencer, C., Antalffy, B., Noebels, J., Armstrong, D., Paylor, R., and Zoghbi, H. (2002). Mice with truncated MeCP2 recapitulate many Rett syndrome features and display hyperacetylation of histone H3. Neuron *35*, 243–254.

Sutcliffe, J.S., Nakao, M., Christian, S., Orstavik, K.H., Tommerup, N., Ledbetter, D.H., and Beaudet, A.L. (1994). Deletions of a differentially methylated CpG island at the SNRPN gene define a putative imprinting control region. Nat. Genet. *8*, 52–58.

Tao, J., Hu, K., Chang, Q., Wu, H., Sherman, N.E., Martinowich, K., Klose, R.J., Schanen, C., Jaenisch, R., Wang, W., and Sun, Y.E. (2009). Phosphorylation of MeCP2 at Serine 80 regulates its chromatin association and neurological function. Proc. Natl. Acad. Sci. USA *106*, 4882–4887.

Woodcock, C.L., Skoultchi, A.I., and Fan, Y. (2006). Role of linker histone in chromatin structure and function: H1 stoichiometry and nucleosome repeat length. Chromosome Res. *14*, 17–25.

Yasui, D.H., Peddada, S., Bieda, M.C., Vallero, R.O., Hogart, A., Nagarajan, R.P., Thatcher, K.N., Farnham, P.J., and Lasalle, J.M. (2007). Integrated epigenomic analyses of neuronal MeCP2 reveal a role for long-range interaction with active genes. Proc. Natl. Acad. Sci. USA *104*, 19416–19421.

Young, J.I., Hong, E.P., Castle, J.C., Crespo-Barreto, J., Bowman, A.B., Rose, M.F., Kang, D., Richman, R., Johnson, J.M., Berget, S., and Zoghbi, H.Y. (2005). Regulation of RNA splicing by the methylation-dependent transcriptional repressor methyl-CpG binding protein 2. Proc. Natl. Acad. Sci. USA *102*, 17551–17558.

Zhang, X., Yazaki, J., Sundaresan, A., Cokus, S., Chan, S.W., Chen, H., Henderson, I.R., Shinn, P., Pellegrini, M., Jacobsen, S.E., and Ecker, J.R. (2006). Genome-wide high-resolution mapping and functional analysis of DNA methylation in arabidopsis. Cell *126*, 1189–1201.

Zhou, Z., Hong, E.J., Cohen, S., Zhao, W.N., Ho, H.Y., Schmidt, L., Chen, W.G., Lin, Y., Savner, E., Griffith, E.C., et al. (2006). Brain-specific phosphorylation of MeCP2 regulates activity-dependent Bdnf transcription, dendritic growth, and spine maturation. Neuron *52*, 255–269.